

# A Fusion Prognostics Strategy for Fuel Cells Operating under Dynamic Conditions: Application to Transportation

Chu Wang <sup>a, b, \*</sup>, Manfeng Dou <sup>a</sup>, Zhongliang Li <sup>b, c, \*\*</sup>, Rachid Outbib <sup>b</sup>, Dongdong Zhao <sup>a</sup> and Bin Liang <sup>d</sup>

<sup>a</sup> School of Automation, Northwestern Polytechnical University, Xi'an 710072, China

<sup>b</sup> LIS Lab (UMR CNRS 7020), Aix-Marseille University, 13397 Marseille, France

<sup>c</sup> FEMTO-ST (CNRS 6174)/FCLAB (CNRS 3539), 90010 Belfort, France

<sup>d</sup> Department of Automation, Tsinghua University, Beijing 100084, China

\* Corresponding author: Chu Wang (e-mail: chu.wang@etu.univ-amu.fr)

\*\* Corresponding author: Zhongliang Li (e-mail: zhongliang.li@lis-lab.fr)

## Abstract

Transportation-oriented proton exchange membrane fuel cells (PEMFC) are attracting much attention, but the strong dynamic operating conditions in transportation applications limit the durability improvement and wide commercialization of fuel cells (FC). Prognostics dedicated to predicting the FC remaining useful life (RUL) can facilitate the early provision of control/maintenance programs to improve durability and reduce costs. However, credible degradation indexes for prognostics cannot be accessed or observed directly from the FC operated under dynamic conditions. Moreover, the long-term prediction performances of the state-of-the-art prognostics models are often not satisfactory. This paper proposes a fusion prognostics strategy to address these challenges. Specifically, the system dynamics is identified by using an electrochemical mechanism model and the degradation indexes are extracted based on the identified model parameters. Subsequently, a reduced-dimensional symbolic representation based long short-term memory networks is developed to predict future degradation indexes. The proposed approach is validated using the long-term accelerated stress test data of a vehicle-oriented PEMFC. The results show that the degradation mechanism model can be used to identify degradation indexes in dynamic operating conditions. Based on the prognostics model, accurate RUL prediction can further be achieved over the extracted degradation indexes.

**Keywords:** Proton exchange membrane fuel cells;

Dynamic conditions;

Electrochemical degradation model;

Degradation indexes;

Failure range;

Remaining useful life

# 1 Introduction

Recently, there is an exponential growth in the focus on all clean energy sources. This comes partly from the distress caused by the fossil fuel shortage and, more seriously, from the exhaust emissions of combustion. Further, reducing carbon emissions in industrial processes and transportation is urgent but challenging [1]. Fuel cells (FC) are expected to alleviate this challenge, thanks to its operation without onboard CO<sub>2</sub> emissions and air pollution [2]. In particular, proton exchange membrane fuel cells (PEMFC) exhibit advantages such as high power density, low starting/running temperature, and high energy conversion efficiency. This allows PEMFC to be suitable for diverse transportation applications, e.g., hybrid/plug-in hybrid vehicles [3,4], heavy-duty trucks [1], buses [5], trains [6], ships [7]. However, the large-scale commercialization of PEMFC still has to face the challenges of durability improvement and cost reduction [8]. For instance, the durability of fuel cells used for low-duty automotive is currently less than 5,000 hours, while the ultimate goal is targeted at 8,000 hours by 2025 [1].

Prognostics and health management (PHM) has the ability to improve FC durability and is considered as one of the superior solutions [9]. In PHM, the accuracy of prognostics plays the deterministic role for the timing of maintenance/control deployment and affects the effectiveness of health management. Prognostics provides the basis for the “Predict”–“Maintain” strategy considered as an alternative of the “Failure”–“Replace” strategy [10]. The former is considered to be better not only to improve the durability, but also to reduce the maintenance cost [11]. The International Organization for Standardization (ISO) defines prognostics as “analysis of the symptoms of faults to predict future condition and residual life within design parameters” [12]. Accordingly, for FC aging prognostics, the core task involves refining the degradation index (DI), predicting the state of health (SoH) and/or the remaining useful life (RUL) [13]. For FC operating in constant conditions, some measurements (such as stack voltage [14,15,16]) can be directly assigned as DI. On the other hand, a suitable DI needs to be extracted for long-term aging prognostics with different dynamics and different DI extraction methods have been studied in literature [17,18,19,20,21]. Specifically, in [17], Bressel et al. estimate the actual SoH and degenerate dynamics using an extended Kalman filter and select the degeneration model parameters as DI. Mezzi et al. assume constant effects of FC system operating conditions and select periodic dynamic voltages as DI [18]. Li et al. use a linear parameter-varying model to extract the virtual steady-state voltage as DI [19,20]. Yue et al. used the multiplicative feature decomposition method to separate the trending part of the system dynamics and designated it as DI [21]. In general, facing variable loads in traffic applications, it is still challenging to effectively decouple the system dynamics from the aging effects and obtain physically interpretable DI.

In the phase of SoH/RUL prediction, the performance of model-free or data-driven based methods is

encouraging. This is due to the fact that such methods adeptly learn and predict the trend characteristics of DI [10,13]. In particular, methods in long short-term memory networks (LSTM) framework have demonstrated their strong performance in short-term SoH prediction [14,15,16,22]. However, LSTM performance becomes unsatisfactory with increased prediction horizon length which was observed and indicated in our previous work [15,23]. Interestingly, the cause of this issue may stem from the powerful “memory” ability of the LSTM, which incorrectly records irrelevant features in the training set. To cope with this issue, Ma et al. in [14] propose to use a fusion model combining the auto-regressive integrated moving average (ARIMA) method with the LSTM. In general, the LSTM based prognostics model still need to be improved in DI long-term prediction while the related studies are extremely limited.

Another key challenge for developing credible FC prognostics tools, especially for PEMFC applied in transportation, is the scarcity of long-term aging data. A recent review [24] comprehensively reports state-of-the-art durability experimental methods for vehicle-oriented PEMFC. The use of the accelerated stress test (AST) not only enables the assessment of FC lifetime, but also effectively reduces the experimental cost and time.

To tackle the above issues, this paper proposes a fusion prognostic strategy for PEMFC in transportation applications, consisting of model-based DI extraction and model-free RUL prediction. Specifically, a time-varying degenerate model based on the FC electrochemical mechanism is developed to track the load dynamics and degradation indexes. The model parameters are identified in variable width intervals, specifying the equivalent resistance and the reconstructed virtual-constant power as DIs, respectively. In the phase of RUL prediction, a reduced-dimensional symbolic representation based LSTM model is used to predict the possible trends of DI. Subsequently, a series of predicted trends form a probability density distribution and RUL is calculated. Finally, the proposed method is validated using a vehicle application-oriented long-term AST dataset.

Sections 2-6 of the article are structured as follows: Section 2 presents the proposed degradation mechanism model. In Section 3, the RUL prediction model and the fusion prognostics strategy are talked about. The experiments used to validate the method are described in Section 4. Section 5 summarizes the prognostic results. The paper is finally concluded in Section 6.

## **2 Model-based dynamics degradation index extraction**

### **2.1 Degradation mechanism model**

Utilizing electrochemical mechanisms such as the models based on polarization curve has been recognized effective to explain FC voltage losses [25]. The polarization curve model contains the voltage losses due to

activation ( $V_{act}$ ), ohmic ( $V_r$ ), and concentration ( $V_{conc}$ ), and is generally expressed as

$$E_{cell} = E_{nernst} - v = E_{nernst} - V_{act} - V_r - V_{conc} \quad (1)$$

where  $E_{cell}$  is the cell voltage,  $E_{nernst}$  is the Nernst voltage representing the open circuit voltage,  $v$  is the global overpotential. A typical polarization curve model is for single cell modeling and generalizes to a  $n$ -cell stack level ( $E_{stack} = n \cdot E_{cell}$ ) ignoring inter-cell differences. However, this model is generally suitable for portraying a PEMFC voltage response to static operating conditions and unable to track transient voltage evolutions in dynamic conditions.

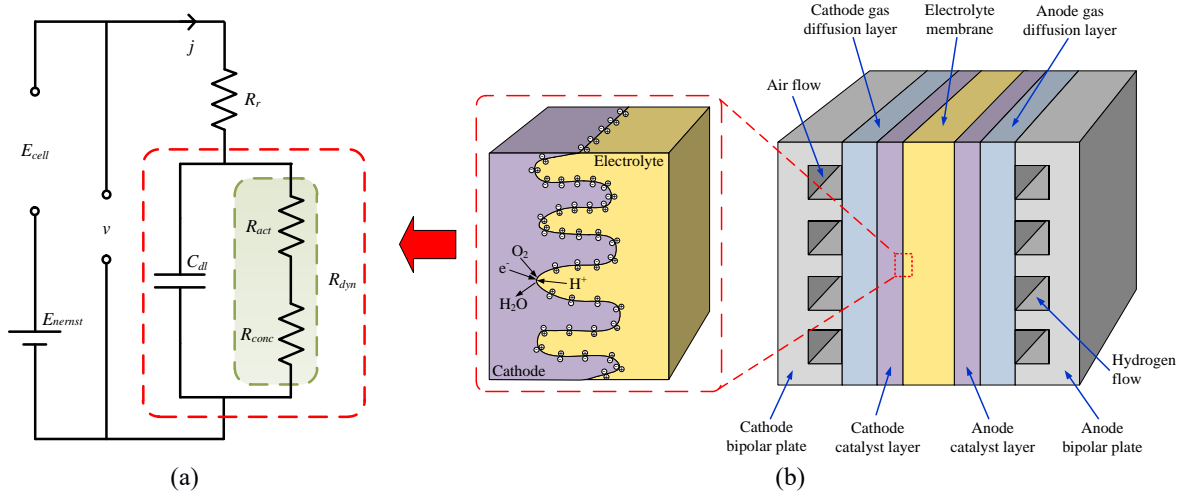


Figure 1. PEMFC electrochemical mechanism schematic:  
(a) equivalent circuit model;  
(b) physical representation of an electrochemical reaction interface.

A typical electrochemical reaction interface is depicted in Figure 1. The electrochemical characteristics of the reaction interface are represented by using a resistor ( $R_{dyn}$ ) and a capacitor ( $C_{dl}$ ) in parallel, as in Figure 1 (a) [26]. Here,  $R_{dyn}$  is called the dynamics resistor to quantify the electrochemical reaction dynamic characteristics. Further it can be decomposed into two resistors  $R_{act}$  and  $R_{conc}$ , which correspond to activation and concentration losses, respectively.  $R_r$  is the resistance corresponding to ohmic losses. Based on this, the three voltage losses can be refined by using the following equations,

$$\begin{cases} V_{act} = jR_{act} + \frac{RT}{\alpha_{a+c}F} \ln\left(\frac{j + j_{loss}}{j_{exch}}\right) \\ V_R = jR_r \\ V_{conc} = jR_{conc} - \frac{RT}{\beta_{a+c}F} \ln\left(1 - \frac{j}{j_{max}}\right) \end{cases} \quad (2)$$

where,  $j$  is the stack current density,  $j_{loss}$  is the crossover current density,  $j_{exch}$  is the exchange current density;  $j_{max}$  is limiting current density.  $R$  is Molar gas constant (8.3145 J/mol/K),  $F$  is Faraday constant

(96485 C/mol).  $\alpha_{a+c}$  is the transfer coefficient,  $\beta_{a+c}$  is a parameter related to the number of electrons transferred in the overall reaction. Both  $\alpha_{a+c}$  and  $\beta_{a+c}$  combine the effects of the anode and the cathode.  $T$  is the operating temperature (thermodynamic temperature) of the cell. Further,  $R_r$  and  $R_{dyn}$  are combined as the equivalent resistor ( $R_{equ}$ ), which represents the overall resistor of the cell, as

$$R_r + R_{act} + R_{conc} = R_r + R_{dyn} = R_{equ} \quad (3)$$

In addition,  $C_{dl}$  is called the double-layer capacitor, which responds to the capacitive characteristics of the reaction interface. As in Figure 1(b), in the electrochemical reaction, a significant charge separation occurs at the reaction interface, with electrons and ions accumulating respectively on the electrode and electrolyte sides. The reaction interface behaves like a capacitor due to the charge separation phenomenon. As shown in the figure, the electrode/electrolyte interface is not smooth, which makes  $C_{dl}$  evident and not ignorable [27].

To specify the dynamics of the equivalent circuit in Figure 1(a), the following equation is utilized.

$$v(t) + R_{dyn}C_{dl} \frac{dv(t)}{dt} = (R_r + R_{dyn})j(t) + R_rR_{dyn}C_{dl} \frac{dj(t)}{dt} \quad (4)$$

Further the one-sided Laplace transform of the left and right sides of equation (4) can be done to obtain the system transfer function, as

$$H(s) = \frac{V(s)}{J(s)} = \frac{R_r s + (R_r + R_{dyn})/R_{dyn}C_{dl}}{s + 1/R_{dyn}C_{dl}} = \frac{b_1 s + b_2}{s + a_1} \quad (5)$$

where  $H(s)$  is considered as a single-input, single-output system.  $a_1$  represents the Laplace variable of the denominator polynomial, and  $b_1$  and  $b_2$  represent the Laplace variables of the numerator polynomial. By feeding the data of both temporal input  $j(t)$  and output  $v(t)$ , the model parameters  $a_1$ ,  $b_1$  and  $b_2$  can be identified. The model parameters  $R_r$ ,  $R_{dyn}$ ,  $C_{dl}$  and  $E_{nernst}$  can further be deduced. The parameter identification process is summarized in Appendix A.

## 2.2 Degradation index extraction based on variable width division

The electrochemical mechanism-based degradation model described above has the ability to characterize the short-term dynamics. Concerning the long-term aging, the electrochemical characteristics of FC change over time and some aging-related parameters can be used to reflect the FC long-term evolution. A DI extraction method based on variable width division is therefore proposed in this paper, as in Figure 2. Specifically, the samples of current density, cell temperature and cell voltage within a time slot are set as

inputs, while the degradation model parameters are set as model identification outputs among which degradation indexes are further selected. It is worth mentioning that the cell temperature is related to the thermal characteristics of FC, and impacts the fuel cell system dynamic behaviors. Therefore, assigning the cell temperature as an input variable facilitates the degradation model to depict the dynamics not covered by the electrochemical mechanism model.

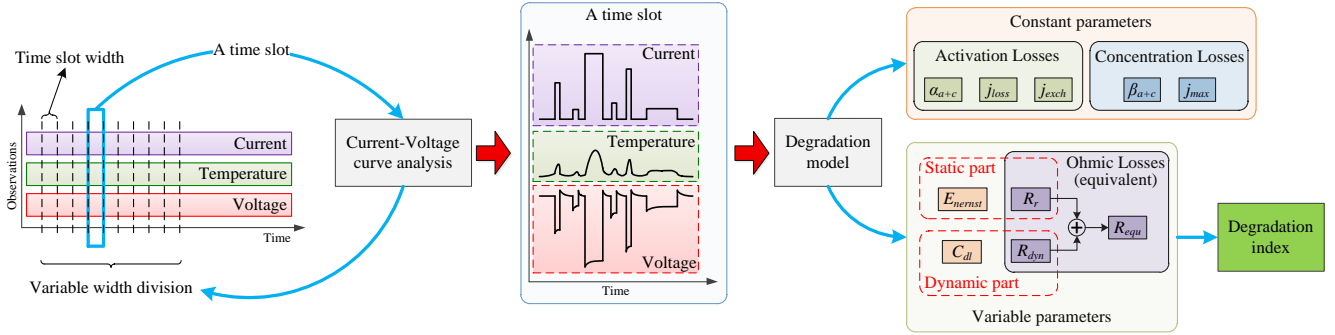


Figure 2. Schematic of variable width division-based degradation index extraction.

Considering that the FC aging is relatively slow, the aging-related parameters can be considered constant in short-term time slots (hourly level). The time slot width should be set in the way that the data within the time slot contain sufficient system dynamics for model identification. As shown in the right side of Figure 2, the variable parameters, i.e.,  $E_{nernst}$ ,  $C_{dl}$ ,  $R_r$ , and  $R_{equ}$  are identified in each time slot via the model identification procedure presented in Appendix A.

Once identified, the parameters that demonstrate evident time-varying characteristics can be considered as the candidates for DI. By further analyzing the trendiness/smoothness of the candidates, the DI suitable for prognostics is selected. In addition, it is possible to consider bringing all the identified parameters into equations (1)-(3) and replacing the original dynamic operating current density with a virtual constant current. Accordingly, the virtual steady-state voltage and power can be calculated. It is thus possible to analyze the output power drop as DI at different loads, especially at nominal power/full load.

### 3 Model-free remaining useful life prediction

#### 3.1 ABBA-LSTM

The Raw-LSTM (a. k. a., Vanilla-LSTM) encounters performance decreasing in long-term prediction, especially when there is a lack of training data concerning the prediction horizon [28]. In the stage of SoH prediction, we use an LSTM model with adaptive Brownian bridge-based aggregation (ABBA-LSTM). Its core idea is expressing the original data with reduced dimensional symbols/letters to improve the sensitivity of Raw-LSTM to trend features. Specifically, ABBA-LSTM can be divided into three parts: representation, prediction, and reconstruction, as in Figure 3.

- Representation:

There are two steps to go through in this part, (1) Compression: which converts an  $n$ -dimensional historical DI (time series  $X$ ) into an  $m$ -dimensional set of segments ( $Q \in \mathbb{R}^m$ ). Next, a time increment ( $len$ ) and a numerical increment ( $inc$ ) of each segment are used to form a tuples-set ( $D$ ). (2) Digitization: after standardization and scaling, an alphabet set ( $L$ ) corresponding to  $k$  clustering categories is constructed. The tuples in  $D$  are expressed using the letters in  $L$  to obtain the character series  $A$  of length  $m$ .

- Prediction:

In the prediction part, a 5-layer LSTM model is utilized, where the input is the character series  $A$ . After two LSTM layers, a fully connected layer and a Softmax layer, the output character series  $B$  contains the predictions for  $p$  time steps.

- Reconstruction:

The predicted character series needs to be recovered as a time series before it is used for FC prognostics, and this part is regarded as the inverse process of representation. Converting character series  $B$  to predicted time series  $Y$  is realized by Inverse-digitization and Inverse-compression.

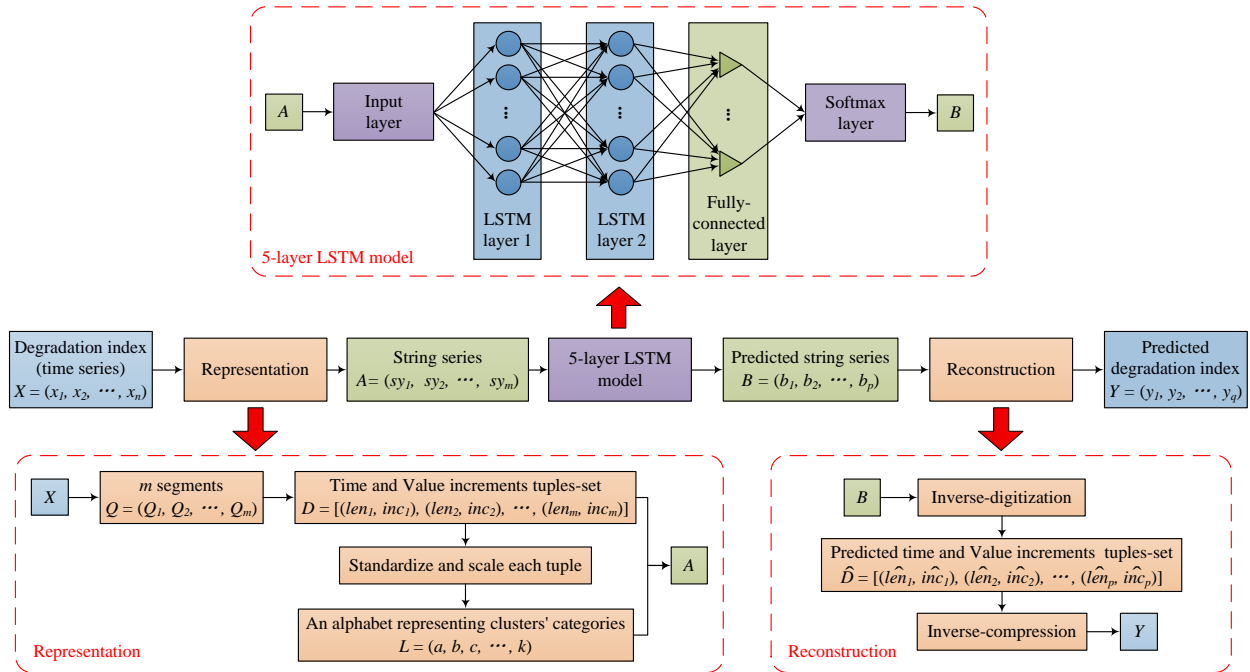


Figure 3. Flowchart of the proposed ABBA-LSTM prognostics model.

To describe this process more clearly, a series of notation marks involved in the ABBA-LSTM prognostics model are shown in Table 1. The detailed operations in each step listed in Figure 3 could be found in our previous work [23].

Table 1 Notation marks during degradation index series conversion

Type	Notation of sets	Remark
Time series	$X = (x_1, x_2, \dots, x_n) \in \mathbb{R}^n$	Historical degradation index
Compression	$D = \left[ \begin{array}{c} (len_1, inc_1), (len_2, inc_2) \\ \dots \\ (len_m, inc_m) \end{array} \right] \in \mathbb{R}^{2 \times m}$	Time and numerical increment tuples-set
Digitization	$L = (a, b, c, \dots, k)$	Alphabet set representing clusters' categories
Digitization	$A = (sy_1, sy_2, \dots, sy_m) \in L^m$ , where $sy_i \in L (i = 1, \dots, m)$	$m$ -dimensional character series
Prediction	$B \in L^p$	$p$ -dimensional predicted set of characters
Inverse-digitization	$\hat{D} \in \mathbb{R}^{2 \times p}$	Predicted increments tuples-set
Inverse-compression	$Y \in \mathbb{R}^q$	Predicted degradation index ( $q$ time steps)

### 3.2 Fusion prognostics strategy

The central goal of fusion prognostics is to predict RUL, firstly by referring back to the ISO definition of RUL, “remaining time before system health falls below a defined failure threshold” [12]. However, there is still no agreement on the definition of the failure threshold (FT) for PEMFC [29]. In some cases, different FTs lead to significantly different RULs [24]. Based on this, a probable failure range (PFR) and a calculable failure range (CFR) are proposed in this paper. Specifically, as shown in Figure 4 (a), the prediction starting point and the extreme point of recoverable fault divide the aging data into three parts: training, prognostics, and invalid data. The range between the expected earliest failure point and the complete failure point (or data ending) is considered as PFR, and the range between the expected earliest failure point and the extreme point of recoverable fault is considered as CFR.

Given a prediction starting time point  $t_0$ , the zoom-in illustration of the prognostic part is shown in Figure 4 (b). By setting  $l$  random initial weight parameters, the ABBA-LSTM model can output a series of predicted degradation index  $\hat{Y} = (Y_1, Y_2, \dots, Y_l), Y_1, Y_2 \dots Y_l \in \mathbb{R}^q$ . The CFR contains  $h$  failure thresholds  $FT = (FT_1, FT_2, \dots, FT_h)$ .

- For the  $i$ -th ( $i = 1, 2, \dots, h$ ) failure threshold  $FT_i$ :

Based on degradation index series  $\hat{Y}$  and  $FT_i$ , a series of RUL ( $RUL_i$ ) can be calculated as

$$\begin{cases} RUL_i = (RUL_{i_1}, RUL_{i_2}, \dots, RUL_{i_j}, \dots, RUL_{i_l}) \in \mathbb{R}^l \\ RUL_{i_j} = t_{i_j} - t_0 \\ RUL_{i_l} = t_{a_i} - t_0 \end{cases} \quad (6)$$

where  $RUL_{i_j}$  is the  $j$ -th ( $j = 1, 2, \dots, l$ ) element in  $RUL_i$ .  $t_{i_j}$  is the operation time at the crossing point of the  $j$ -th degradation index  $Y_j$  and  $FT_i$ .  $t_{a_i}$  is the operation time at the crossing point of



actual DI and  $FT_i$ .  $RUL_{a_i}$  is the actual RUL value. Estimate the probability density distribution ( $P_i$ ) based on the RUL series  $RUL_i$ , as

$$f(RUL_{P_i}) = P_i \quad (7)$$

where  $RUL_{P_i}$  corresponds to the RUL values of the horizontal coordinate of  $P_i$ . The final predicted RUL value ( $R\tilde{U}L_i$ ) at  $FT_i$  can be obtained as

$$R\tilde{U}L_i = \operatorname{argmax}_{RUL_{P_i} \in RUL_i} f(RUL_{P_i}) \quad (8)$$

where the  $\operatorname{argmax}_{x \in S} f(x)$  represent arguments  $x$  for which  $f(x)$  attains its largest value.

- For the failure threshold series  $FT$ :

Each failure threshold contained in  $FT$  corresponds to a predicted RUL value as described above, and  $h$  predicted RUL values constitute a predicted RUL series  $R\hat{U}L = (R\tilde{U}L_1, R\tilde{U}L_2, \dots, R\tilde{U}L_h) \in \mathbb{R}^h$ .

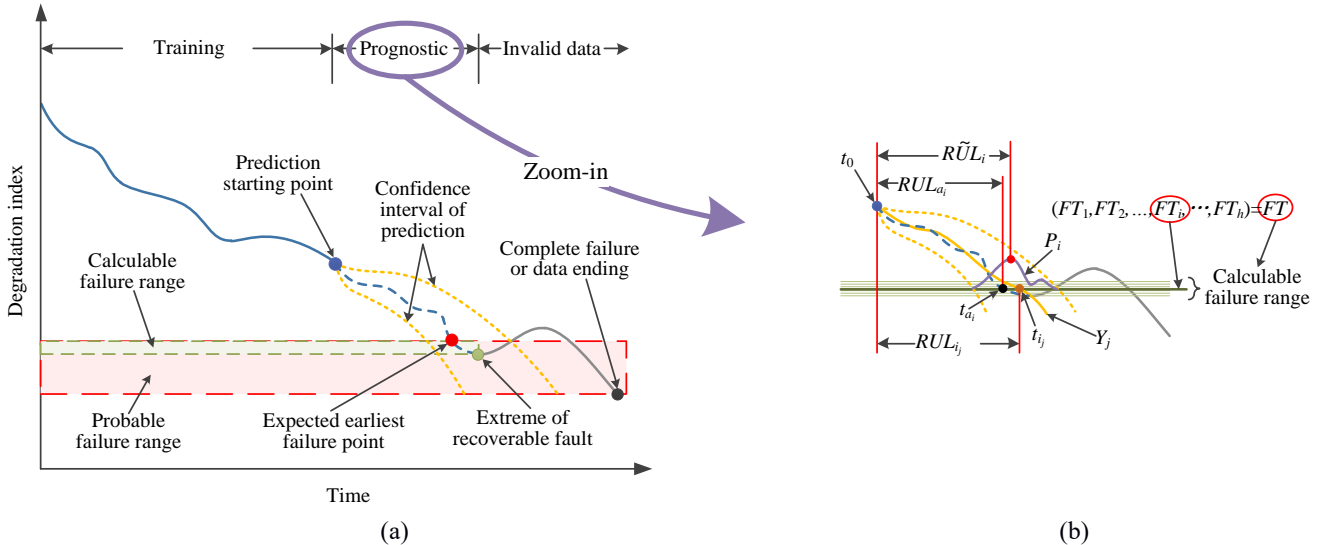


Figure 4. Schematic of fusion prognostics:

(a) segmentation of degradation index (data set), and failure ranges;

(b) when prediction starting point is  $t_0$ , zoom-in prognostic part and predict remaining useful life.

## 4 Vehicle-oriented long-term accelerated stress test experiments

To properly validate the proposed fusion prognostics method, long-term dynamic aging experimental data from a vehicle-oriented commercial PEMFC single cell is used [30]. Specifically, a test station with integrated control and observation was used to deploy the aging experiment, and to activate the PEMFC before performing the test. The relative humidity of the cathode and anode was regulated by the built-in

humidifier of the test station. A peripheral water-cooling system was used to handle the operating temperature of PEMFC. The main technical parameters of the PEMFC are listed in Table 2, where the cathode/anode inlet pressures and relative humidity, as well as the operating temperature are set to the desired optimal values.

Table 2 Dynamic aging test conditions

Items	Values			
Active surface (cm <sup>2</sup> )	25			
Hydrogen inlet-pressure (KPa)	110			
Air inlet-pressure (KPa)	110			
Operating temperature (°C)	85			
Hydrogen relative humidity (%)	50			
Air relative humidity (%)	80			
Full load current (A)	35.6			
Load currents involved in dynamic load cycles (A)	0;	1.78;	4.45;	9.51;
	10.4;	14.85;	20.75;	29.65

This aging experiment can be considered as an In-situ accelerated stress test (AST) [24], which was designed with reference to the New European Driving Cycle (NEDC) [30]. As shown in Figure 5, each cycle lasted for 1,181 s, including the urban condition (performed 4 times) and the suburban condition (performed 1 time). Nine different load currents (0-100%) are involved as shown in Table 2. The entire aging experiment consisted of 3,076 cycles, accounting for approximately 1,008 hours. A polarization curve test was performed prior to the start of the overall aging experiment. Subsequently, the AST was suspended every 50 hours and resumed until the end of the polarization curve test (non-shutdown). In addition, every 100 hours, a planned shutdown of 12 hours was executed to simulate the shutdown-condition of the actual vehicle. It is worth mentioning that typically the shutdown comes with a performance recovery of the PEMFC. This is realistic, but it inevitably causes fluctuations in DI, making the prognostics challenging.

During the aging experiments, the test station and peripheral equipment encountered some anomalies, which are referred to as abnormal operations in this paper. As in Figure 6(a), the inlet/outlet pressure of hydrogen was set at the optimal value of 110 KPa, however, in practice, some significant fluctuations occurred. Among them,

- Point A is a sharp oscillation of the inlet pressure that occurred at around 156 hours, corresponding to the shutdown-like voltage dip in Figure 5(a).
- Point B is the frequent and more violent hydrogen supply anomalies starting at around 634 hours, especially in the blue dashed box in Figure 6(a).

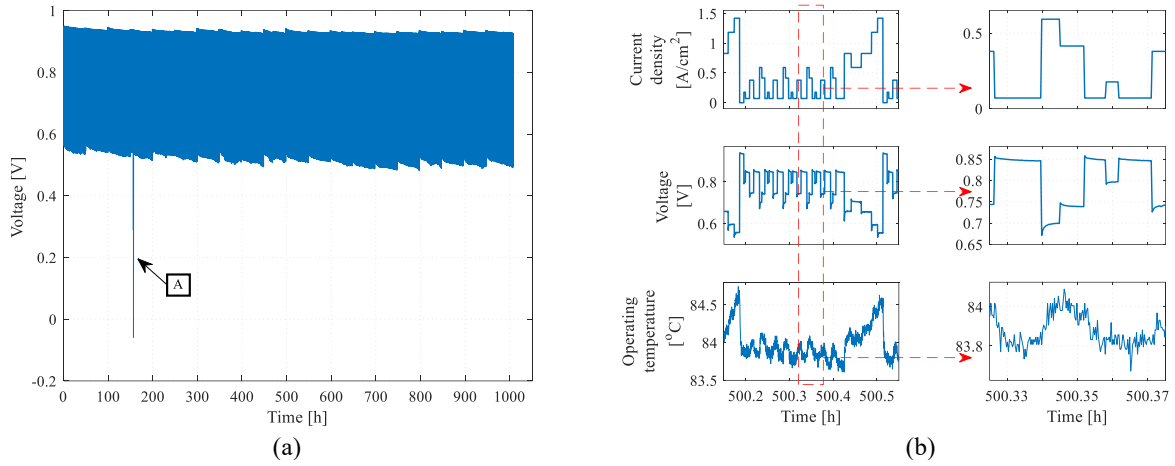


Figure 5. Cyclic dynamic loading for accelerated stress testing:  
 (a) overall dynamic voltage;  
 (b) around 500 hours, current density, voltage and operating temperature in one cycle, and zoom-in details.

The current density-voltage scatterplot for different time periods are shown in Figure 6(b)-(e). (b) is overall (0-1008 hours) plot, which contains the long-term degradation and anomalous operations. (c), (d), and (e) are the current density-voltage scatterplots for 0-1, 500-501, and 1007-1008 hours. It is observed that (c)-(e) show a voltage drop over time, which reflects the degradation of the performance. Distinct from the typical polarization curves, the data points in (c)-(e) are more divergent due to the inclusion of short-term (transient) dynamics. In these cases, the degeneration model proposed in this paper can be used to treat the dynamics.

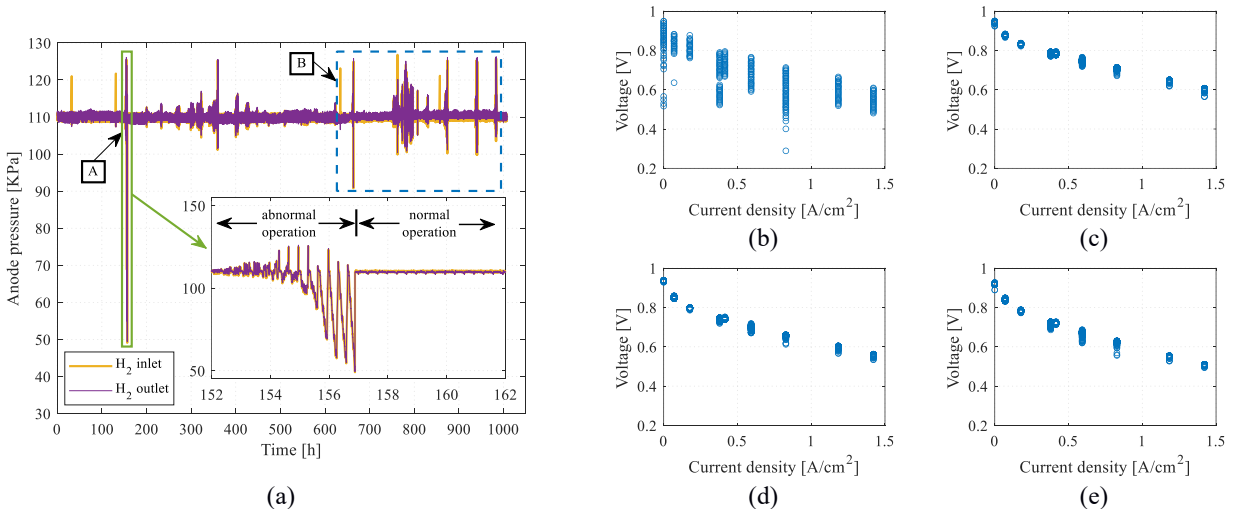


Figure 6. Anode gas pressure conditions and current density-voltage scatterplots:  
 (a) schematic of the relationship between anode gas pressure and abnormal operation;  
 Current density-voltage scatterplot in,  
 (b) overall (0-1008 hours); (c) 0-1 hours; (d) 500-501 hours; (e) 1007-1008 hours.

## 5 Prognostics results evaluation and discussion

### 5.1 Evaluation criteria

In this paper, two metrics are used to evaluate the hybrid prognostics method, relative error (RE) and prognostic horizon (PH). Among them, RE is given by

$$RE = \frac{|x - \hat{x}|}{x} \cdot 100\% \quad (9)$$

where  $x$  can be the actual single-cell voltage ( $E_{cell}$ ) or the actual remaining useful life ( $RUL_{ai}$ );  $\hat{x}$  corresponds to the predicted single-cell voltage ( $\hat{E}_{cell}$ ) or the predicted remaining useful life ( $R\tilde{U}L_i$ ).

Subsequently, the predicted RUL is further evaluated using PH, the definition of which differs from those proposed in [29,31]. In this paper, PH is defined using a Trust Area (TA), which is the area between the upper/lower trustworthiness boundaries parallel to the actual RUL. In the CFR, the  $i$ -th ( $i = 1, 2, \dots, h$ ) failure threshold ( $FT_i$ ) corresponds to the  $TA_i$  and the  $PH_i$  as follows

$$\begin{cases} RUL_i - t_{FT_i} \cdot \alpha_{low} \leq TA_i \leq RUL_i + t_{FT_i} \cdot \alpha_{up} \\ PH_i = t_{FT_i} - t_{1st} \end{cases} \quad (10)$$

where  $\alpha_{low}$  and  $\alpha_{up}$  are used to adjust the tolerance of TA, the smaller they are the tighter the TA (and the smaller the range of TA). In this paper,  $\alpha_{low}$  and  $\alpha_{up}$  are set to 15% and 5%, respectively.  $t_{FT_i}$  is the operation time corresponding to the intersection of  $FT_i$  and the actual DI.  $t_{1st}$  denotes the earliest time point after which the predicted RULs are all within the set TA. Larger PH is, more sufficient time is guaranteed for control/maintenance and the more effective the prognostics.

### 5.2 Evaluation of extracted degradation index

Based on the analysis for the current density-voltage scatterplot in Section 4, in this paper, equal interval division is chosen for the DI extraction. The width of each time slot is set to the duration of 3 dynamic cycles (about 1 hour). In Table 3 the identified parameters are listed, along with the type of voltage losses to which they belong.

In Figure 7, the identified variable parameters are shown. By introducing all identified parameters into equations (1)-(3) and setting the operating current at 35.6 A, the equivalent full-load power ( $P_{equ}$ ) is calculated and illustrated in Figure 7(f). In overall, almost all the variable parameters show a significant jump at point A, this is caused by a severe fault in the hydrogen supply. Meanwhile, there is a clear change of the trend after point B, which can be considered as an effect from the change in hydrogen supply behavior. There

are some obvious outlier points in  $C_{dl}$  and the trend characteristics are not obvious. In addition, all other variable parameters show different levels of trend characteristics until point B. To be specific,  $E_{nernst}$  and  $P_{equ}$  appear to possess generally decreasing trends, but  $P_{equ}$  looks smoother.  $R_r$ ,  $R_{dyn}$  and  $R_{equ}$  imply generally increasing trends, with  $R_{equ}$  showing a more clearly monotonous trend. Moreover, considering that both  $R_{equ}$  and  $P_{equ}$  are the parameters that characterize the overall situation with physical interpretation, they are designated as  $DI_1$  and  $DI_2$ , respectively.

Table 3 Parameter identification results

Parameter	Value/Range	Overpotential losses
$\alpha_{a+c}$	0.74	Activation
$j_{loss}$ (mA/cm <sup>2</sup> )	10	Activation
$j_{exch}$ (mA/cm <sup>2</sup> )	9	Activation
$\beta_{a+c}$	0.13	Concentration
$j_{max}$ (A/cm <sup>2</sup> )	3.539	Concentration
$C_{dl}$ (mF/cm <sup>2</sup> )	64 to 464	Activation & Concentration
$R_{dyn}$ ( $\Omega$ cm <sup>2</sup> )	-0.007 to 0.053	Activation & Concentration
$R_r$ ( $\Omega$ cm <sup>2</sup> )	0.03 to 0.08	Ohmic
$R_{equ}$ ( $\Omega$ cm <sup>2</sup> )	0.0344 to 0.1002	Ohmic (nominal)
$E_{nernst}$ (V)	0.923 to 0.967	-

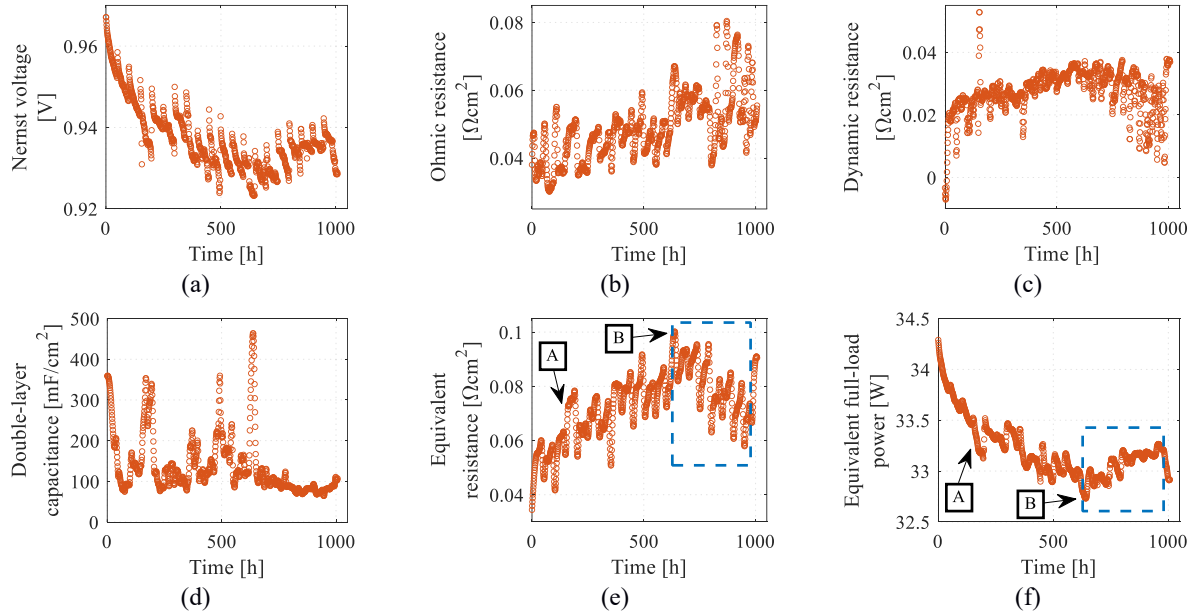


Figure 7. Parameters identification:

- (a) Nernst voltage ( $E_{nernst}$ ); (b) Ohmic resistor ( $R_r$ ); (c) dynamic resistor ( $R_{dyn}$ );  
(d) double-layer capacitor ( $C_{dl}$ ). (e) equivalent resistor ( $R_{equ}$ ); (f) equivalent full-load power ( $P_{equ}$ ).

The final output of the degradation mechanism model is the single cell voltage. Thus, the cell voltage values calculated using the identified model are compared with the actual measurements to evaluate the model identification performance. As an example, Figure 8 (a) and (b) show the comparison corresponding to a dynamic cycle around 500 hours. Figure 8 (a) shows that the operating voltages and the reconstructed voltages can match well to the practical measurements. Figure 8 (b) shows the current density-voltage plot in which the overall match is satisfactory. Furthermore, to quantitatively evaluate the model performance, the relative error ( $RE_E$ ) in terms of single-cell voltage is calculated using equation (9) and illustrated in Figure 8(c). Observations for the aging test are sampled at 1 Hz, so the  $RE_E$  is calculated over more than 3.6 million data points. The average  $RE_E$  is less than 1%, which demonstrates the effectiveness of the proposed model and model identification method.

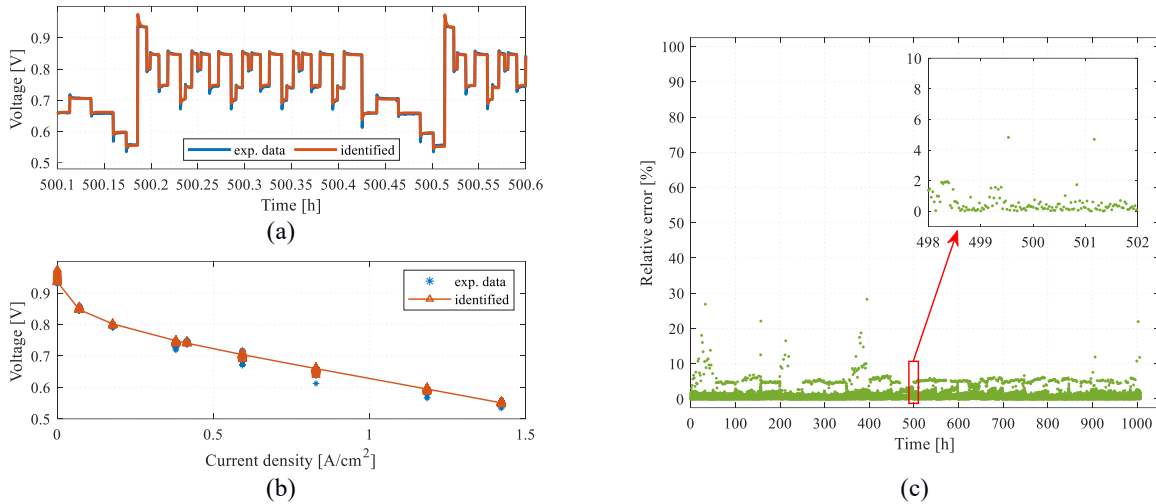


Figure 8. Evaluation of dynamic load identification performance:  
(a) identification of the cell voltage;  
(b) current density-voltage plot of identification results;  
(c) relative error of identification results.

### 5.3 Evaluation of predicted remaining useful life

In evaluating the performance of the proposed RUL prediction method, the prediction starting points and failure range are set based on the analysis of  $DI_1$  and  $DI_2$ , as in Figure 9. In particular, a change in operational behavior after point B is considered. As a consequent change in the degradation trend is observed after B, the DI after the maximum/minimum point near B (approximately hour 640) is set as invalid. For the useful DI, RUL predictions are deployed at 50-hour intervals from about 50 hours to about 500 hours. Meanwhile, a CFR consisting of a series of failure thresholds is set in place of a single failure threshold. For  $DI_1$ , the CFR is 0.0961-0.1001  $\Omega\text{cm}^2$ ; while the CFR for  $DI_2$  is set to 32.74-32.82 W.

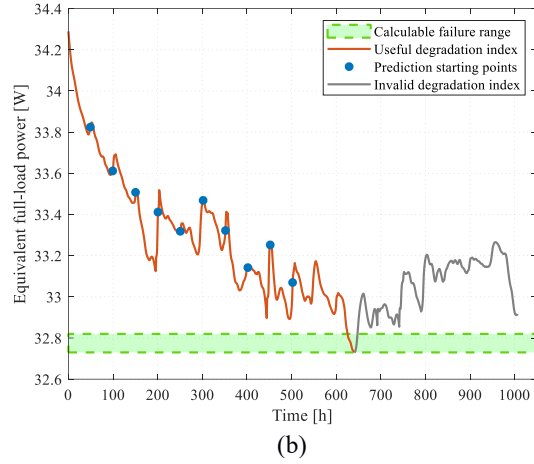
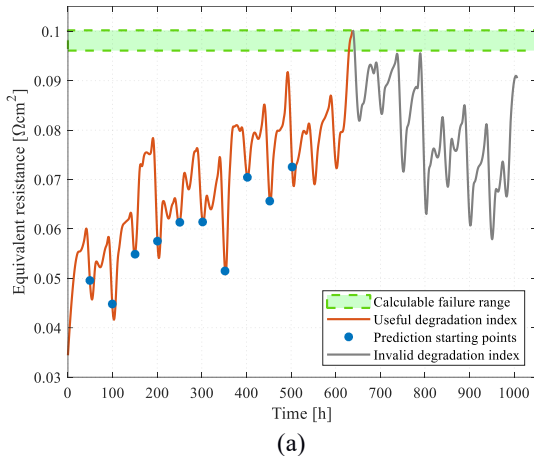


Figure 9. Degradation index and failure range for prognostics:  
 (a) equivalent resistor ( $DI_1$ );  
 (b) equivalent full-load power ( $DI_2$ ).

For  $DI_1$ , the performance of the proposed method in terms of RUL prediction is evaluated as shown in Figure 10. In the first two test points, the predicted RUL does not enter the TA. This is mainly due to the fact that the training data in the early stage are not sufficient to capture the global evolution trend. With increased training data, the prediction error gradually decreases and predicted RUL enters the TA. The calculated PH exceeds 350 hours on different FTs. If the full useful lifetime is set to 640 hours, this means that the PH exceeds 50% of it. On the other hand, in Figure 10(e), the prediction performance is quantitatively evaluated using equation (9). Overall, the prediction errors maintain a high stability when FT varies. Moreover, the average relative error in the CFR is 15.5%.

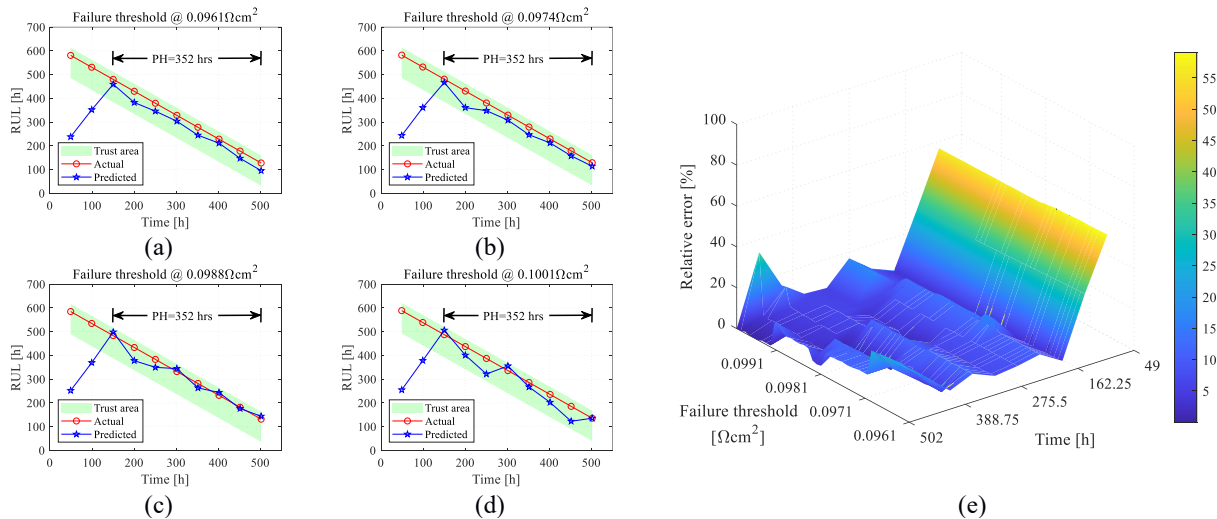


Figure 10. For  $DI_1$ , RUL prediction performance and evaluation at different failure thresholds (FT):  
 (a) prognostic horizon at  $FT=0.0961 \Omega\text{cm}^2$ ; (b) prognostic horizon at  $FT=0.0974 \Omega\text{cm}^2$ ;  
 (c) prognostic horizon at  $FT=0.0988 \Omega\text{cm}^2$ ; (d) prognostic horizon at  $FT=0.1001 \Omega\text{cm}^2$ ;  
 (e) relative error of the CFR ( $0.0961\text{-}0.1001 \Omega\text{cm}^2$ ).

The same performance evaluation is deployed on  $DI_2$ , as in Figure 11. Thanks to  $DI_2$  being smoother, the prediction performance is better than  $DI_1$  overall. For different FTs, PHs are greater than 400 hours which accounts for more than 60% of the full useful lifetime. In the best case, PH exceeds 450 hours, which means that satisfactory prognostic results can be given with only 50 hours aging data. On the other hand, the performance of the relative error is stable within the CFR. Then the average relative error in the CFR is 11.4%.

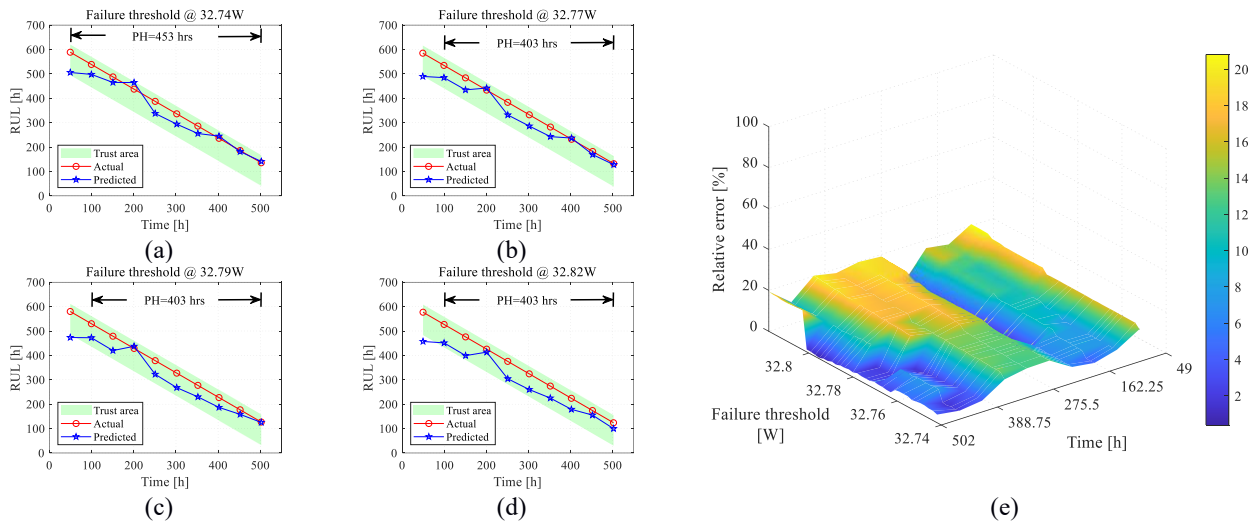


Figure 11. For  $DI_2$ , RUL prediction performance and evaluation at different failure thresholds (FT): (a) prognostic horizon at FT=32.74 W; (b) prognostic horizon at FT=32.77 W; (c) prognostic horizon at FT=32.79 W; (d) prognostic horizon at FT=32.82 W; (e) relative error of the CFR (32.74-32.82 W).

## 6 Conclusion

In this work, a fusion prognostics strategy is proposed for predicting the remaining useful life of fuel cells. A degradation mechanism model is used to handle the dynamic operating conditions of the fuel cell and extract the degradation indexes that can be used for prognostics. In addition, the proposed method is validated using the accelerated stress test/dynamic load cycle aging test data of a vehicle-oriented PEMFC. The results show that the proposed degradation mechanism model can effectively track both the dynamics caused by load transitions and the aging-related parameter variation. The average relative error of the model output is less than 1%. Furthermore, two different degradation indexes, i.e., equivalent resistance and full power, are extracted and the ABBA-LSTM RUL prediction model is evaluated in the set failure region of the two degradation indexes respectively. The results show that the prognostic horizon exceeds 60% of the useful full lifetime can be achieved, and the relative error of RUL prediction can reach at 11.4%. The proposed fusion strategy has the ability to handle long-term prognostics that are full of dynamics in automobile applications. In the future work, we aim to identify and remove the unnatural aging component of the degradation index to improve the aging prognostic performance.



## Acknowledgement

This work was supported in part by the China Scholarship Council (CSC) under Grant [grant number 201906290107].

## Appendix A

In general, the refined choice of filter ( $L(s)$ ) is used to cope with the disturbances embedded in the system when estimating the system variables [32].

$$L(s) = \frac{1}{A(s)} \quad (\text{A.1})$$

In fact,  $A(s)$  is the denominator of  $H(s)$ , for which the unknown part is replaced by the estimated value. Based on this, the following equation is obtained after filtering equation (4).

$$\begin{aligned} L(s)v'(t) &= -a_1L(s)v(t) + b_1L(s)j'(t) + b_2L(s)j(t) + L(s)e(t) \\ &= \varphi^T(t)\theta + L(s)e(t) \end{aligned} \quad (\text{A.2})$$

where  $v'(t)$  and  $j'(t)$  correspond to the first order derivatives of the variables,  $e(t)$  is the disturbance of the system, and  $\varphi(t)$  and  $\theta$  are as follows,

$$\begin{cases} \varphi(t) = [-L(s)v(t), L(s)j'(t), L(s)j(t)]^T \\ \theta = [a_1, b_1, b_2]^T \end{cases} \quad (\text{A.3})$$

Considering that typically  $e(t)$  is not necessarily white noise, the Instrumental Variable (IV) method is chosen in order to reduce the estimation bias. The predicted output ( $\hat{v}(t)$ ) will constitute the instrument vector ( $\zeta(t)$ ),

$$\zeta^T(t) = [-L(s)\hat{v}(t), L(s)j'(t), L(s)j(t)] \quad (\text{A.4})$$

The parameters are subsequently estimated using the following equation,

$$\hat{\theta} = \left( \sum_{i=1}^N \zeta^T(t_i)\varphi(t_i) \right)^{-1} \sum_{i=1}^N \zeta^T(t_i)[L(s)v'(t_i)] \quad (\text{A.5})$$

where  $\hat{\theta}$  represents the estimated parameters [32].

## References

- [1] T. Ramsden, "2019 Annual Progress Report: DOE Hydrogen and Fuel Cells Program," United States, 2020. <https://www.osti.gov/biblio/1660255>.
- [2] European Commission, "A hydrogen strategy for a climate-neutral Europe," Brussels, Belgium, 2020. [https://ec.europa.eu/energy/sites/ener/files/hydrogen\\_strategy.pdf](https://ec.europa.eu/energy/sites/ener/files/hydrogen_strategy.pdf).
- [3] M. Yue, S. Jemei, R. Gouriveau, and N. Zerhouni, "Review on health-conscious energy management strategies for fuel cell hybrid electric vehicles: Degradation models and strategies," *International Journal of Hydrogen Energy*, vol. 44, no. 13, pp. 6844-6861, 2019, <https://doi.org/10.1016/j.ijhydene.2019.01.190>.
- [4] X. Hao, Y. Yuan, H. Wang, M. Ouyang, "Plug-in hybrid electric vehicle utility factor in China cities: Influencing factors, empirical research, and energy and environmental application," *eTransportation*, 2021, <https://doi.org/10.1016/j.etrans.2021.100138>.
- [5] Z. Hu, L. Xu, J. Li, M. Ouyang, Z. Song, et al., "A reconstructed fuel cell life-prediction model for a fuel cell hybrid city bus," *Energy Conversion and Management*, vol. 156, pp. 723-732, 2018, <https://doi.org/10.1016/j.enconman.2017.11.069>.
- [6] H. Peng, Z. Chen, K. Deng, S. Dirkes, C. Ünlübayir, et al., "A comparison of various universally applicable power distribution strategies for fuel cell hybrid trains utilizing component modeling at different levels of detail: From simulation to test bench measurement," *eTransportation*, vol. 9, 2021, <https://doi.org/10.1016/j.etrans.2021.100120>.
- [7] A. Pfeifer, P. Prebeg, N. Duić, "Challenges and opportunities of zero emission shipping in smart islands: A study of zero emission ferry lines," *eTransportation*, vol. 3, 2020, <https://doi.org/10.1016/j.etrans.2020.100048>.
- [8] W. Gao, Z. Hu, H. Huang, L. Xu, C. Fang, et al., "All-condition economy evaluation method for fuel cell systems: System efficiency contour map," *eTransportation*, vol. 9, 2021, <https://doi.org/10.1016/j.etrans.2021.100127>.
- [9] M. Jouin, R. Gouriveau, D. Hissel, M.-C. Péra, N. Zerhouni, "Degradations analysis and aging modeling for health assessment and prognostics of PEMFC," *Reliability Engineering & System Safety*, vol. 148, pp. 78-95, 2016, <https://doi.org/10.1016/j.ress.2015.12.003>.
- [10] A. Jacome, D. Hissel, V. Heiries, M. Gerard, and S. Rosini, "Prognostic methods for proton exchange membrane fuel cell under automotive load cycling: a review," *IET Electrical Systems in Transportation*, vol. 10, no. 4, pp. 369-375, 2020, <https://doi.org/10.1049/iet-est.2020.0045>.
- [11] T. Sutharssan, D. Montalvao, Y. K. Chen, W.-C. Wang, C. Pisac, and H. Elemara, "A review on prognostics and health monitoring of proton exchange membrane fuel cell," *Renewable and Sustainable Energy Reviews*, vol. 75, pp. 440-450, 2017, <https://doi.org/10.1016/j.rser.2016.11.009>.
- [12] ISO, "ISO 13381-1:2015 Condition monitoring and diagnostics of machines — prognostics — Part 1: General Guidelines," 2015. <https://www.iso.org/standard/51436.html>.
- [13] H. Liu, J. Chen, D. Hissel, J. Lu, M. Hou, and Z. Shao, "Prognostics methods and degradation indexes of proton exchange membrane fuel cells: A review," *Renewable and Sustainable Energy Reviews*, vol. 123, 2020, <https://doi.org/10.1016/j.rser.2020.109721>.
- [14] R. Ma et al., "Data-Fusion Prognostics of Proton Exchange Membrane Fuel Cell Degradation," *IEEE Transactions on Industry Applications*, vol. 55, no. 4, pp. 4321-4331, 2019, <https://doi.org/10.1109/tia.2019.2911846>.
- [15] C. Wang, Z. Li, R. Outbib, D. Zhao, and M. Dou, "Proton Exchange Membrane Fuel Cells Prognostic Strategy Based on Navigation Sequence Driven Long Short-term Memory Networks," in *IECON 2020 The 46th Annual Conference of the IEEE Industrial Electronics Society*, 2020: IEEE, pp. 3969-3974, <https://doi.org/10.1109/IECON43393.2020.9255373>.
- [16] F. K. Wang, X. B. Cheng, and K. C. Hsiao, "Stacked long short-term memory model for proton exchange membrane fuel cell systems degradation," *Journal of Power Sources*, vol. 448, Feb 2020, Art no. 227591, <https://doi.org/10.1016/j.jpowsour.2019.227591>.
- [17] M. Bressel, M. Hilairret, D. Hissel, and B. Ould Bouamama, "Remaining Useful Life Prediction and Uncertainty Quantification of Proton Exchange Membrane Fuel Cell Under Variable Load," *IEEE Transactions on Industrial Electronics*, vol. 63, no. 4, pp. 2569-2577, 2016, <https://doi.org/10.1109/tie.2016.2519328>.

- [18] R. Mezzi, N. Yousfi-Steiner, M. C. Péra, D. Hissel, and L. Larger, "An Echo State Network for fuel cell lifetime prediction under a dynamic micro-cogeneration load profile," *Applied Energy*, vol. 283, 2021, <https://doi.org/10.1016/j.apenergy.2020.116297>.
- [19] Z. L. Li, S. Jemei, R. Gouriveau, D. Hissel, N. Zerhouni, and Ieee, "Remaining useful life estimation for PEMFC in dynamic operating conditions," in *2016 Ieee Vehicle Power and Propulsion Conference, (IEEE Vehicle Power and Propulsion Conference, 2016)*, <https://doi.org/10.1109/VPPC.2016.7791762>.
- [20] Z. Li, Z. Zheng, and R. Outbib, "Adaptive Prognostic of Fuel Cells by Implementing Ensemble Echo State Networks in Time-Varying Model Space," *IEEE Transactions on Industrial Electronics*, vol. 67, no. 1, pp. 379-389, 2020, <https://doi.org/10.1109/tie.2019.2893827>.
- [21] M. Yue, Z. Li, R. Roche, S. Jemei, and N. Zerhouni, "A Feature-based Prognostics Strategy For PEM Fuel Cell Operated Under Dynamic Conditions," in *Prognostics and System Health Management Conference (PHM-Besancon), Besancon, FRANCE, 2020*, pp. 122-127, <https://doi.org/10.1109/PHM-Besancon49106.2020.00026>.
- [22] J. Zuo et al., "Deep learning based prognostic framework towards proton exchange membrane fuel cell for automotive application," *Applied Energy*, vol. 281, 2021, <https://doi.org/10.1016/j.apenergy.2020.115937>.
- [23] C. Wang, Z. Li, R. Outbib, M. Dou, and D. Zhao, "Symbolic deep learning based prognostics for dynamic operating proton exchange membrane fuel cells," *Applied Energy*, vol. 305, 2022, <https://doi.org/10.1016/j.apenergy.2021.117918>.
- [24] J. Zhao and X. Li, "A review of polymer electrolyte membrane fuel cell durability for vehicular applications: Degradation modes and experimental techniques," *Energy Conversion and Management*, vol. 199, 2019, <https://doi.org/10.1016/j.enconman.2019.112022>.
- [25] F. J. Asensio, J. I. San Martín, I. Zamora, G. Saldaña, and O. Oñederra, "Analysis of electrochemical and thermal models and modeling techniques for polymer electrolyte membrane fuel cells," *Renewable and Sustainable Energy Reviews*, vol. 113, 2019, <https://doi.org/10.1016/j.rser.2019.109283>.
- [26] Y. Qi, M. Espinoza-Andaluz, M. Thern, T. Li, and M. Andersson, "Dynamic modelling and controlling strategy of polymer electrolyte fuel cells," *International Journal of Hydrogen Energy*, vol. 45, no. 54, pp. 29718-29729, 2020, <https://doi.org/10.1016/j.ijhydene.2019.09.178>.
- [27] R. O'hayre, S.-W. Cha, W. Colella, and F. B. Prinz, *Fuel cell fundamentals*. John Wiley & Sons, 2016, <https://doi.org/10.1002/9781119191766>.
- [28] S. Elsworth and S. Güttel, "Time series forecasting using LSTM networks: A symbolic approach," *arXiv preprint arXiv:2003.05672*, 2020. <https://arxiv.org/abs/2003.05672>.
- [29] M. Jouin et al., "Estimating the end-of-life of PEM fuel cells: Guidelines and metrics," *Applied Energy*, vol. 177, pp. 87-97, 2016, <https://doi.org/10.1016/j.apenergy.2016.05.076>.
- [30] J. Zuo et al., "Long-term dynamic durability test datasets for single proton exchange membrane fuel cell," *Data Brief*, vol. 35, p. 106775, Apr 2021, <https://doi.org/10.1016/j.dib.2021.106775>.
- [31] A. Saxena et al., "Metrics for evaluating performance of prognostic techniques," in *International Conference on Prognostics & Health Management, 2008*, <https://doi.org/10.1109/PHM.2008.4711436>.
- [32] L. Ljung, "Experiments with identification of continuous time models," in *IFAC Proceedings Volumes (IFAC-PapersOnline), 2009*, vol. 15, PART 1 ed., pp. 1175-1180, <https://doi.org/10.3182/20090706-3-FR-2004.0209>.